Electronic supplementary materials *Mendeleev Commun.*, 2021, **31**, 24-26

Composite nanoparticles with titania–poly(*N*-vinylamide) core–shell structure

Galina M. Kuz'micheva, Olesya I. Timaeva, Irina P. Chikhacheva, Roman V. Svetogorov, Ratibor G. Chumakov, Natalia V. Sadovskaya, Pavel V. Dorovatovskii and Raisa P. Terekhova

Synthesis. The synthesis included the following stages: hydrolysis of titanyl sulfate hydrate (Sigma Aldrich) at (0.95 mol×L^{-1}) either in the presence of PVP (0.18 mol×L^{-1}, sample 1) or PVCL[S1] (0.14 mol×L^{-1}, sample 2) for 60 min at 90±2°C, the addition of the 0.10 mol×L^{-1} aqueous KOH solution, centrifugation (15 min, 3000 rpm), separation of the supernatant fluid by centrifugation (3000 rpm, 10 min), and precipitate drying in a drying oven for 1 h at 90±2°C. The PVP (BASF) and PVCL[S1] polymers with molecular masses (M_w) of 1×10^6 Da were used. The commercial Hombikat UV100 and Hombifine N were synthesized by sol-gel and sulfate methods, respectively (Sachtleben Chemie GmbH).

X-ray diffractometry (XRD). The samples were investigated by the powder diffraction method using a «Belok» endstation established on a beam from the bending magnet of the Kurchatov synchrotron radiation source: the «transmission» scheme with the registration of the spatial pattern with the help of the CCD Rayonix SX165 two-dimensional detector (2048×2048), wavelength λ = 0.95445 Å. Intensity–diffraction angle dependence $I(2\theta)$ is found by averaging over diffraction cones («caking»).[S2] The crystalline structure (unit cell parameters, coordinates of oxygen atoms, the atomic displacement parameters of all atoms, and the occupancies of titanium and oxygen crystallographic positions) was refined using Rietveld profile refinement principles with the Jana2006 software.[S3] The reflection profiles were approximated by the pseudo-Voigt function. The error factor (R_p) for all the refinements performed was less than 2%. The average crystallite sizes and magnitudes of microstresses (Table S1) were determined from all reflections by the Williamson-Hall method[S4] for spherical nanoobjects[S5,6] with taking into account the instrumental broadening, obtained from measurement of the certified $Na_2Ca_3Al_2F_{14}$ powder standard. The refinement of occupation factors of titanium and oxygen sites was performed by various methods. The oxygen occupancy was refined at a fixed titanium occupancy (it was decreased for sample 2), and the titanium occupancy was refined at a fixed oxygen occupancy (it was decreased for all samples), or occupancies of two crystallographic sites of the structure refined simultaneously (they were decreased only for sample 2) when refining the atomic displacement parameters.

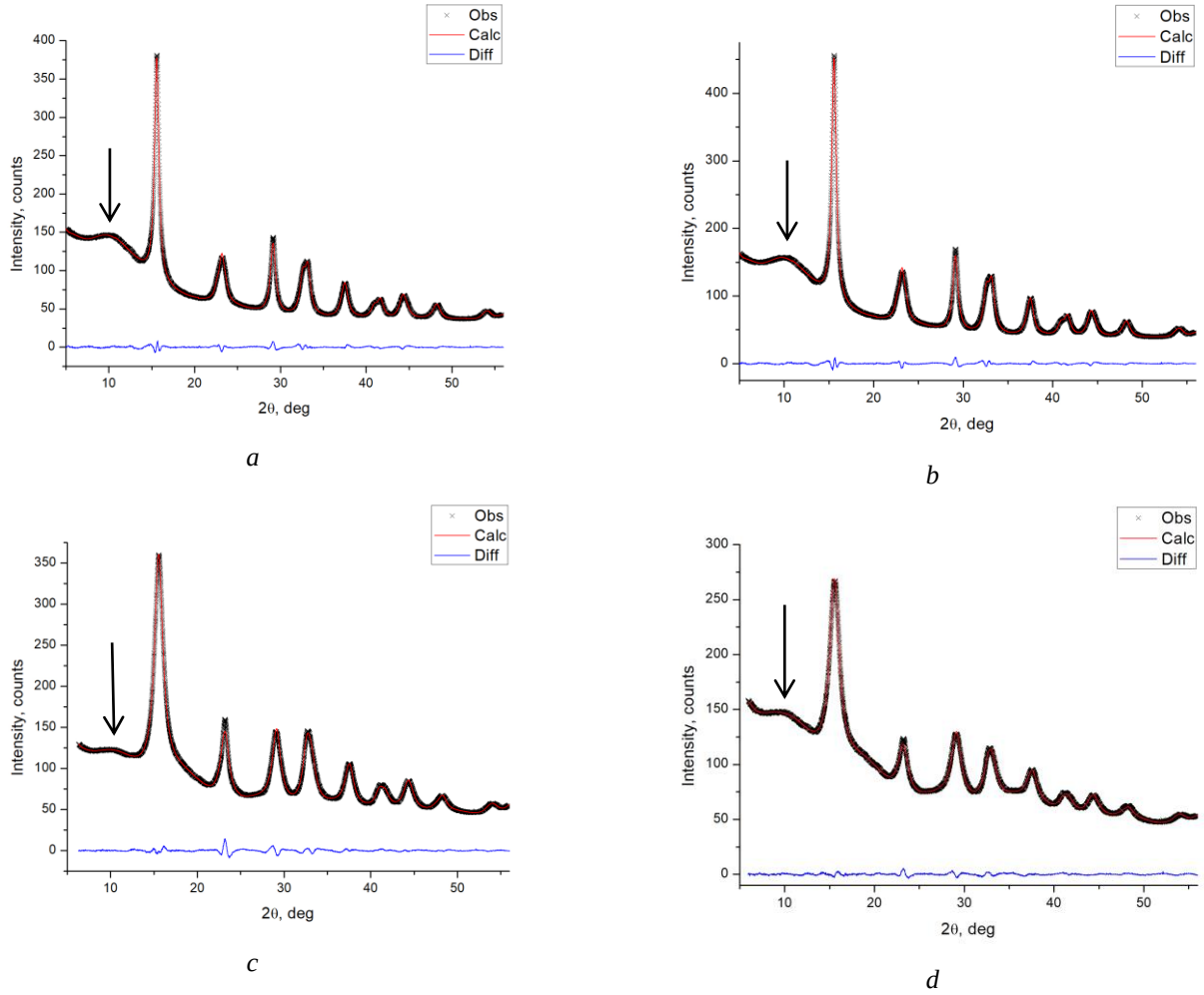

Figure S1 Rietveld refinement (observed, calculated and difference patterns) of the X-ray powder diffraction pattern of (*a*) Hombifine N, (*b*) Hombikat UV100, (*c*) sample 1 and (*d*) sample 2. The arrows indicate the diffuse peak of $TiO_{2-x}(OH)_{2x}\times yH_2O$) and/or $(TiO)(HSO_4)_x(OH)_y$

Table S1 Results of refining the crystalline structure of studied samples

		Hombifine N[S7]	Hombikat UV100	Sample 1	Sample 2[S7]
Space group		$I4_1/amd$			
***a*, Å**		3.79170(6)	3.79234(6)	3.79310(13)	3.79468(11)
***c*, Å**		9.4965(4)	9.4994(4)	9.4896(5)	9.4785(5)
Scherrer size, nm		12.5	12.8	4.47	4.79
Microstrains, %		1.83	1.77	0.95	1.91
Ti	**Occ**	0.966(8)	0.968(8)	0.923(14)	0.887(9)
	U11	0.0052(4)	0.0043(4)	0.0254(6)	0.0238(7)
	U22	0.0052(4)	0.0043(4)	0.0254(6)	0.0238(7)
	U33	0.0070(9)	0.0078(9)	0.0040(13)	0.0082(9)
O	**Occ**	1	1	1	0.984(9)
	U11	0.0100(18)	0.0096(17)	0.047(4)	0.0161(18)
	U22	0.0238(13)	0.0210(13)	0.021(2)	0.0063(13)
	U33	0.061(3)	0.061(3)	0.053(4)	0.148(3)
	z	0.20919(10)	0.20933(10)	0.21250(8)	0.21312(9)
Ti-O		1.9379(2)	1.9376(2)	1.9288(3)	1.9265(3)
		1.9905(10)	1.9918(9)	2.0157(8)	2.0164(9)
O-Ti-O		101.56(3)	101.52(3)	100.63(2)	100.44(3)
		78.44(3)	78.48(3)	79.37(2)	79.56(3)
		156.89(4)	156.96(4)	158.75(3)	159.13(4)
		92.300(8)	92.285(7)	91.948(6)	91.880(6)
$2\theta_{min}$–$2\theta_{max}$, $\Delta 2\theta$ (º)		4.83-56.47, 0.008	4.95-56.47, 0.008	6.342-56.47, 0.008	5.942-56.47, 0.008
$\chi^2/R_{wp}/R_{exp}$		0.027/0.014/0.085	0.019/0.015/0.109	0.026/0.017/0.106	0.009/0.010/0.105
Refined composition		$(Ti_{0.966(8)}\square_{0.034})O_2$	$(Ti_{0.968(8)}\square_{0.032})O_2$	$(Ti_{0.923(14)}\square_{0.077})O_2$	$(Ti_{0.887(9)}\square_{0.113})(O_{1.968(18)}\square_{0.032})$

The IR absorption spectra of powders were recorded using KBr pellets in the 4000–400 cm^{-1} frequency range with a Bruker Equinox 55 Fourier-transform infrared spectrometer (Germany). The spectra were recorded with the resolution of 2 cm^{-1}, the wavenumber accuracy was 0.1 cm^{-1}.

The broad absorption band around 3000–3600 cm^{-1} was attributed to physically adsorbed water coupled with Ti-OH surface groups on the surface of nanoparticles of samples 1 and 2 (Figure S3). The amount of water is somewhat larger in sample 1 judging by the ratio of the maximal band intensity at 3427 cm^{-1}, by the hydrogen bond. Bands at 2927 and 2854 cm^{-1} belong to valence vibrations of CH_2 groups in the main polymer chain.[S8] Bands of nonplanar deformation vibrations of OH groups presented in a range of 1618–1648 cm^{-1} for the samples.[S9] However, these bands intersect with stretching vibration bands of the N-C=O amide group of polymers.[S10] The appearance of bands in a region of 1000–1250 $см^{-1}$ is caused by asymmetric and antisymmetric stretching vibrations of SO_4^{2-} groups connected with Ti^{4+}.[S11] These bands are much more intense (by a factor of ~2) for sample 1 when compared with sample 2. The peak observed in pure PVP at 1683 cm^{-1}, which is due to C=O bonds,[S12] is red-shifted to 1631 cm^{-1}, which can result from the possible interaction of the carbonyl oxygen with the titanium ion.

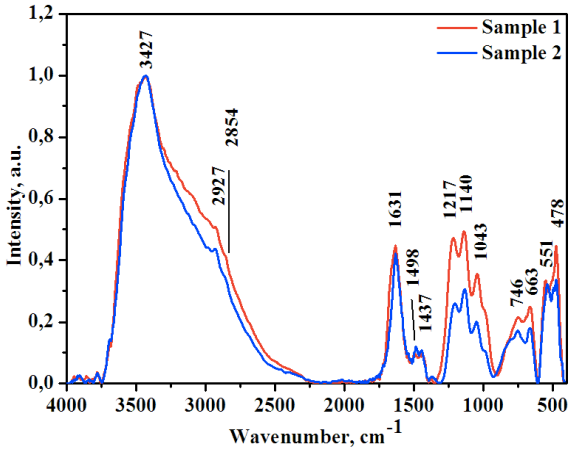

Figure S2 IR spectra of samples 1 and 2

Elemental CHNS analysis of the samples was performed using a Euro Vector EA-3000 CHNS analyzer (Italy). The determination error of the amount was as follows: C < 0.3%, H and N < 0.1%, S < 0.2%.

X-ray photoelectron spectroscopy (XPS). XPS spectra were recorded using a PHOIBOS 150 spectrometer (Germany), Al*K*α radiation. The powder particles were pressed into the surface of the copper foil (when recording the spectra, the rarefaction in the spectrometer chamber was no larger than 2×10^{-9} Torr; the source powder was 100 W). The spectra were recorded in a constant transmission energy mode (120 eV for the general spectra recorded with a step of 0.5 eV and 20 eV for the spectra of separate lines with a step of 0.05 eV). The spectra were calibrated using peaks Au $4f_{7/2}$ (83.8 eV) and Ag $3d_{5/2}$ (367.9 eV) of gold and silver, respectively, fastened on a holder.

Samples 1 and 2 contain an equal amount of elemental O in the form of OH groups (~14 at %) (the band at 531.7 eV[S13] in Figure S3*b,d*) similarly to Hombifine N and Hombikat UV100 commercial samples (~27 at %). The total content of elements in the samples under study is presented in Table S2.

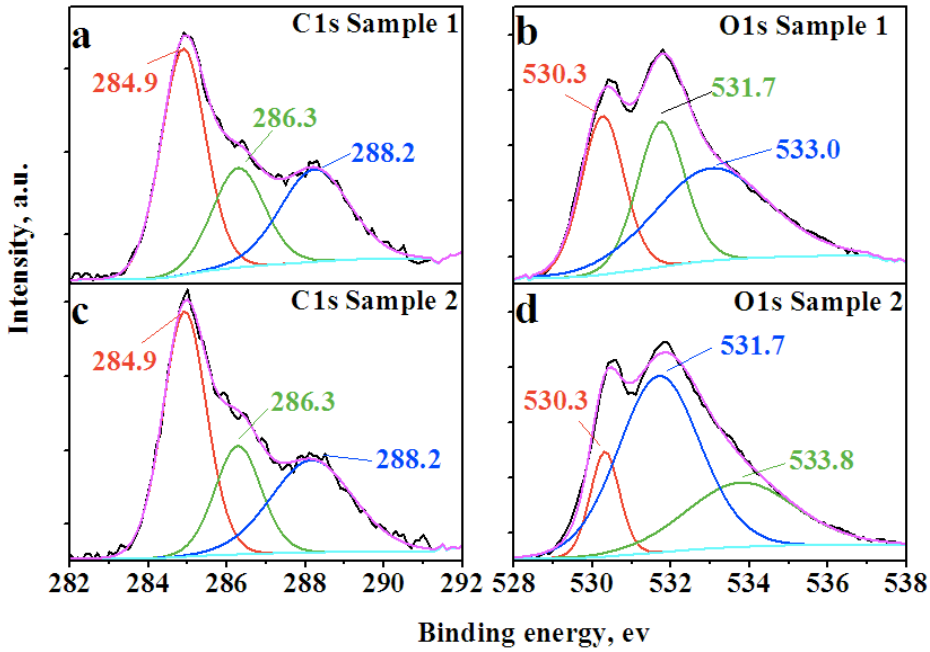

Figure S3 (*a*) C1s and (*b*) O1s XPS-spectra of sample 1; (*c*) C1s and (*d*) O1s XPS-spectra of sample 2

Table S2 Content of elements in the samples under study according to CHNS-analysis and XPS data

Sample	Content, at %								
	CHNS-analysis				XPS				
	N	C	H	S	N	C	O	S	Ti
PVCL	9.568	64.906	8.744	0	-[a]				
PVP	11.123	56.706	7.610	0	-[a]				
Hombifine N	-[a]	-[a]	-[a]	-[a]	0.6	20.20	61.12	-[b]	18.14
Hombikat UV100	-[a]	-[a]	-[a]	-[a]	-[b]	33.20	55.29	-[b]	11.52
Sample 1	0.603	2.912	1.230	3.709	1.12	36.25	50.78	6.12	4.92
Sample 2	0.471	3.257	1.375	3.829	1.00	41.24	48.78	3.77	4.28

[a] - was not determined; [b] - element is not found

Three bands are present in C1s spectra (Figure S3*a,c*) of synthesized samples: ~285 eV (C in the C–C form), 286 eV (C in the N–C=O form), and 289 eV (C in the O–C=O form), which belong to PVCL and PVP polymers and the carbon-containing surface contamination.[S14] Most samples that have been exposed to the atmosphere will have a detectable quantity of adventitious carbon contamination. Argon sputtering may remove adventitious carbon. C1s spectrum for the contamination typically has C–C and O–C=O components,[S14] i.e., the XPS method is ineffective for determining the carbon content on the surface of samples 1 and 2 with PVCL and PVP.

The surface of Hombifine N and Hombikat UV100 nanoparticles contain C (more for Hombikat UV100 due to a larger specific surface area), which are uncontrolled impurities that are almost always detected by the XPS method. Comparison of the C content in commercial samples with samples 1 and 2 indicates the presence of C from PVCL and PVP. According to the XPS data, synthesized samples have N in the form of C–N groups in an amount smaller than 3 at % with the higher content in sample 1 compared to sample 2 (Table S2), and the larger amount of S in the form of SO_4^{2-} is present on the surface of sample 1 with PVP compared to sample 2 with PVCL (Table S2).

The detailed analysis of the fine structure of titanium lines ($Ti2p_{3/2}$) showed the presence of the low-energy component in the spectrum (the peak at the energy of 458.2 eV). Given the absence of other chemical components in the sample composition excluding titanium, oxygen, and carbon evidence the presence of oxygen vacancies in the near-surface sample layer (Figure S4).

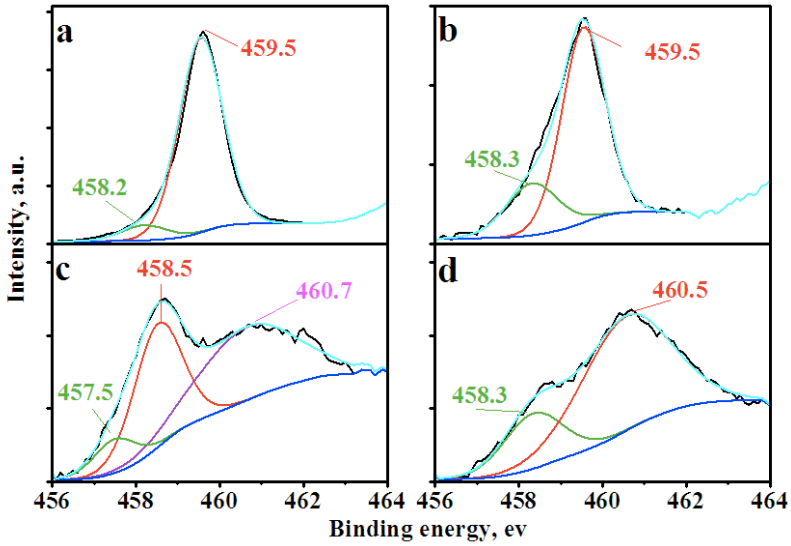

Figure S4 $Ti2p_{3/2}$ spectra of (*a*) Hombifine N, (*b*) Hombikat UV100, (*c*) sample 1 and (*d*) sample 2

A considerable distinction in the number of vacant states is observed for certain samples (Hombikat UV100, sample 2) comparing the XPS data with the X-ray diffraction data (Table S1). It can evidence the arrangement of oxygen vacancies preferentially on the surface of sample nanoparticles given the high surface sensitivity of the XPS method. Indeed, the fraction of atoms situating in nanoparticles in a thin near-surface layer is considerably higher when compared with microparticles. The free nanoparticle surface is a sink of an infinite capacity for defects including point defects. This effect substantially rises with small particle sizes, which can lead to the escape of most of structural defects on the surface.

Scanning electron microscopy (**SEM**) of the samples was performed with a high-resolution JSM 7500F scanning electron microscope (Japan).[S15] To analyze microstructural photographs by plotting the particle-size distribution, we used «The software for processing the photographic images of electron microscopy».[S16] The elemental composition of the samples was determined by energy-dispersive X-ray

microanalysis (**EDX**) in a region with lateral sizes from 2×2 to 100×100 μm using an INCA Penta FET-x3 energy-dispersive X-ray microanalysis system (Oxford Instruments, UK) coupled with a scanning electron microscope. The analyzer was equipped with a nitrogen-cooled silicon-lithium detector; the resolution was 129 eV for carbon. The detector was calibrated based on CoK_α radiation from the cobalt metal standard. The elemental composition was measured at electron beam energy of 15 keV. The information depth (~3.1 μm) was evaluated using the «Depth of X-ray Production» program.

Although PVCL is a thermally sensitive polymer with the phase transition temperature (liquid-solid, tangle-globule) in limits of physiological temperatures of 32–34 °C,[S17] no clear presence of globules was found at the synthesis temperature of 90 °C in PVCL-containing sample 2 (Figure S5*c*). Previously, we determined the size of PVCL globules of 40–50 nm using SEM.[S18] Sample 2 has less than 2% of particles with such sizes, which can be the globules of free PVCL (Figure S5*d*).

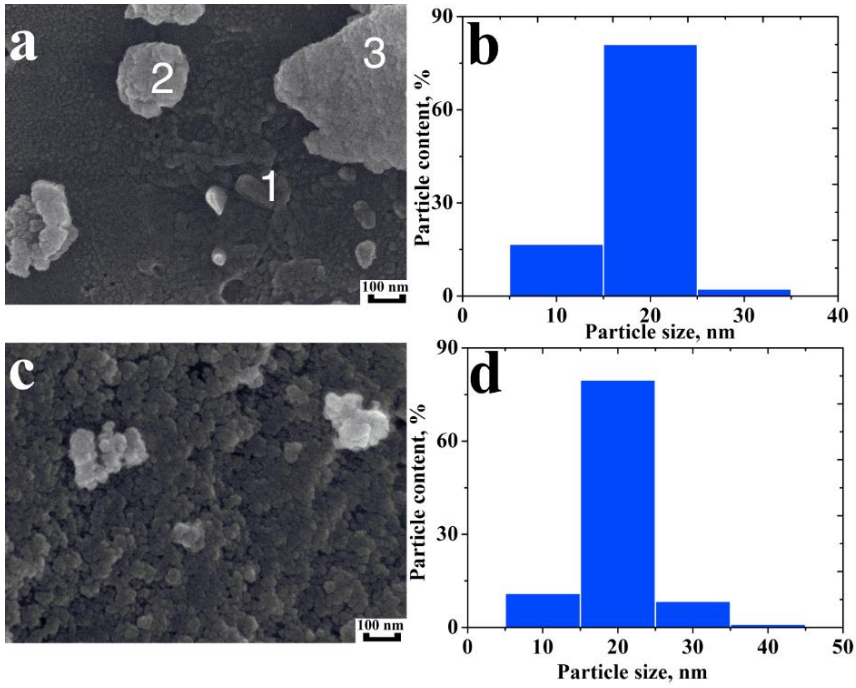

Figure S5 Photographs of the microstructure and the particle size distribution of (*a*,*b*) sample 1 and (*c*,*d*) sample 2. The regions with the predominant content of the polymer without Ti (1), the Ti without polymer (2), the core (associates of nanoparticles)/shell (polymer) (3). Associates with > 100 nm size are not presented in the histograms.

Despite the complexities of the simultaneous investigation of core/shell structures by SEM and EDX methods, which is in the difference in scales of applying these methods (SEM-nanometers, EDX-micrometers), it is established by the EDX method that the elements referring both to anatase (Ti and O) and polymers (C, N, and O) are distributed over the surface of the samples under study inhomogeneously (we investigated 10 regions with sizes from 2×2 to 10×10 μm). The results of studying the most typical regions are presented in Table S3.

Table S3 Content of elements (at %) in the samples under study according to the EDS data

Element	Sample 1			Sample 2[S7]	
	Region with polymer without Ti	Region with Ti without polymer	Core/shell region	Region with Ti without polymer	Core/shell region
C	34.97	12.46	44.44	13.76	29.27
N	63.63	0.00	17.12	0.00	10.49
O	0.00	61.08	28.64	70.32	52.90
S	0.42	6.15	1.47	0.83	3.26
Ti	0.00	29.81	7.24	15.08	6.25

Three regions can be distinguished for sample 1 with PVP: the region with the polymer without Ti, the region with Ti without polymer, and the core-shell region. No regions containing only polymer elements were found for sample 2 with PVCL, i.e., it is not excluded that PVCL polymer completely participates in the formation of core-shell particles. The absence of elemental N was considered as the absence of polymer in the region under study. The content of elements in the samples under study according to the EDX data without corrections to the surface contamination is presented in Table S3. The large complexity in studying the core (associates)/shell (polymer) structures is in the fact that SEM studies the structure morphology at a nanolevel, while EDS does it at a microlevel. The presence of S atoms (~2 at %) – traces of the $TiOSO_4 \times xH_2O$ precursor (Table S1) – is characteristic of both samples.

Microbiological studies of the antimicrobial activity (**AMA**) in the dark were performed against the following microorganisms: *Staphylococcus aureus*, *Escherichia coli*, and *Candida albicans* using an agar diffusion method. The suspension of bacteria containing 10^7–10^8 CFU in 1 ml was seeded as a «lawn» in Petri dishes on the Mueller-Hinton agar in an amount of 0.2 ml. The holes were made on the surface of agar seeded with cultures of microorganisms (through a thin-walled cylinder with a diameter of 6–8 mm), in which the samples of the test material are placed. The caps were placed into a thermostat at 37 °C for 24 h. The results were evaluated by the phenomenon of the growth delay of microorganisms around the discs: the diameter of growth delay of microbes around the discs was determined using a ruler including the diameter of the disc itself.[S19] The degree of sensitivity of microorganisms to the samples under study was established based on the magnitude of the growth absence zone of microorganisms. Microbiological studies were performed in a box preliminarily irradiated by a UV lamp for sterilization of test-cultures before seeding onto nutrient media.

Photocatalytic activity (**PCA**) was estimated using model photocatalytic degradation reactions of the dyes methyl orange (**MO**) and methylene blue (**MB**). The initial concentrations of aqueous MO and MB solutions (C_0) were 17 mg L^{-1}, respectively; the mass concentration of the suspended photocatalyst was 0.5 g L^{-1}. The ratio of the current concentration of the dye (after UV light irradiation of the mixture with a 26 W mercury lamp for τ min) to the initial concentration (C/C_0) was monitored by spectrophotometry following the changes in the intensity of the absorption band of MO at a wavelength of about 490–510 nm and the band of MB at 662 nm.[S20] The activities of different photocatalysts were compared based on the

reaction rate constant, which was evaluated graphically from the constructed plots. The rate constant (k) was calculated as the slope of the linear semilogarithmic plot of the change in the substrate concentration C/C_0 versus the irradiation time. In all cases, the validity of the linear approximation of the kinetic curves was 5%.

The photocatalytic activity is determined by the lifetime of photogenerated charge carriers and their transfer rate over the sample surface. When analyzing publications[S21-25] we can also distinguish other characteristics, which affect the catalytic activity: the composition of samples, phases, and surface; the size of nanoparticles of all levels; and the degree of crystallinity and developed specific surface. Herewith, the last two factors are mutually contradictory: the presence of the developed specific surface implies a large number of defects in the structure and a low degree of crystallinity and, consequently, decreases the PCA. Therefore, to increase the PCA, it is important to hold the balance between the above-mentioned factors.

The cause of the different photocatalytic behavior of samples 1 and 2 can be different supramolecular structures of PVCL and PVP. The «liquid-solid» phase separation temperature (the lower critical dissolution temperature of ~32–34°C)[S17] enters the range of the selected synthesis temperature of sample 2. When attaining this temperature, the PVCL polymer, being in the form of a coil, precipitates already in the form of a globule with the capture of a certain amount of anatase nanoparticles already formed at this temperature. It follows from here that the surface of globules and their associates for sample 2, when compared with sample 1, is depleted with nanodimensional anatase containing active OH groups responsible for the PCA. It is confirmed by the data of Tables S3 and S4.

References

S1 Yu. E. Kirsh, T. M. Karaputadze and V. I. Shumskii, USSR Inventor's Certificate № 1613446 A1, 1990.

S2 S. N. Sulyanov, A. N. Popov and D. M. Kheiker, *J. Appl. Cryst.,* 1994, **27,** 934.

S3 M. Dusek, V. Petricek and L. Palatinus, *Acta Cryst.*, 2006, **62,** s46.

S4 W. H. Hall, *Proc. Phys. Soc.*, 1949, **62,** 741.

S5 G. M. Kuz'micheva, *Fine Chem. Technol.,* 2015, **10,** 5.

S6 A. A. Gainanova, G. M. Kuz'micheva and I. G. Vasilyeva, *Russ. Chem. Bull.*, 2018, **67,** 1350.

S7 O. Timaeva, V. Nikolaichik, R. Svetogorov and G. Kuz'micheva, *Z. Kristallogr. Cryst. Mater.,* 2020, 4-5, https://doi.org/10.1515/zkri-2019-0051

S8 P. Singh, A. Srivastava and R. Kumar, *J. Polym. Sci., Part A-1: Polym. Chem.*, 2010, **50,** 1503.

S9 K. Nakamoto, *Infrared and raman spectra of inorganic and coordination compounds: Part A: theory and applications in inorganic chemistry* (New York: John Wiley & Sons), 2008.

S10 Sh. Sun and P. Wu, *J. Phys. Chem. B,* 2011, **115,** 11609.

S11 X. Wang, J. C. Yu, P. Liu, X. Wang, W. Su and X. Fu, *J. Photochem. Photobiol. A,* 2006, **179,** 339.

S12 R. Chadha, V. Kapoor and A. Kumar, *J. Sci. Ind. Res.*, 2006, **65,** 459.

S13 O. I. Timaeva, I. P. Chihacheva, G. M. Kuz'micheva, L. V. Saf'yanova, R. G. Chumakov and R. P. Terekhova, *Appl. Nanosci.*, 2018, **8,** 1729.

S14 J. F. Moulder, W. F. Stickle, P. E. Sobol and K. D. Bomben, *Handbook of x-ray photoelectron spectroscopy* (USA: Perkin Elmer), 1992.

S15 L. N. Obolenskaya, G. M. Kuzmicheva, E. V. Savinkina, A. V. Zhilkina, N. V. Sadovskaya, N. A. Prokudina and V. V. Chernyshev, *Russ. Chem. Bull.*, 2012, **61,** 2049.

S16 G. M. Kuzmicheva, V. V. Podbel'sky, O. I. Timaeva and L. R. Ishakova, *Program for processing IR spectra and correlation of absorption bands with standards.* Patent № 2017611789.

S17 Yu. E. Kirsh, *Water soluble poly-N-vinylamides. Synthesis and physicochemical properties* (Chichester: John Wiley and Sons), 1998.

S18 I. P. Chihacheva, O. I. Timaeva, G. M. Kuz'micheva, A. V. Dorohov, N. A. Lobanova, S. V. Amarantov, V. V. Podbel'skiy, V. E. Serousov and N. V. Sadovskaya, *Crystallogr. Rep.*, 2016, **61,** 421.

S19 B. M. Dotsenko, S. V. Biryukova and T. I. Tamm, *Methodical recommendations for experimental (preclinical) study of drugs for topical treatment of purulent wounds* (Moscow: Moscow), 1989.

S20 E. V. Savinkina, L. N. Obolenskaya, G. M. Kuz'micheva, A. V. Dorokhov and A. Yu. Tsivadze, *Dokl. Phys. Chem.*, 2011, **441,** 224.

S21 H. Kominami, Sh. Murakami, J. Kato, Y. Kera and B. Ohtani, *J. Phys. Chem. B*, 2002, **106**, 10501.

S22 C. G. Skoutelis, M. Antonopoulou, A. E. Giannakas, Y. Deligiannakis and I. K. Konstantinou, *J. Adv. Oxid. Technol.*, 2014, **17**, 202.

S23 A. Y. Ahmed, T. A. Kandiel, T. Oekermann and D. Bahnemann, *J. Phys. Chem. Lett.*, 2011, **2**, 2461.

S24 D. Beydoun, R. Amal, G. Low and S. J. McEvoy, *J. Nanopart. Res.*, 1999, **1**, 439.

S25 D. W. Bahnemann, *Isr. J. Chem.*, 1993, **33**, 115.